Updating Orthophotos around Gas Pipelines based on "Cloud Control" Photogrammetry

Lei Qin[1], Yawen Liu[1], Xinbo Zhao[1], Yansong Duan[1,2,*]

[1] School of Remote Sensing and Information Engineering, Wuhan University, Wuhan China - qinlei@whu.edu.cn,
liuyawen@whu.edu.cn, simple_zhao@whu.edu.cn, ysduan@whu.edu.cn
[2] Hubei Luojia Laboratory, Wuhan China

Key Words: Long-distance Natural Gas Pipelines, Orthophoto Updating, "Cloud Control" Photogrammetry, UAV, Image Registration.

Abstract

As a clean energy source, natural gas is widely used and primarily transported through long-distance pipelines. Regular maintenance and inspection of long-distance gas pipelines are crucial tasks. Due to the extensive coverage and distance of these pipelines, the workload is enormous. It is necessary to first identify areas of change, which can be carried out using multiple sets of orthophotos produced by unmanned aerial vehicles (UAVs). However, UAV images have small footprints and significant geometric distortions, requiring a large number of ground control points (GCPs) for accurate positioning. Measuring these points in the field is challenging and time-consuming, becoming a key factor limiting the rapid production of orthophotos. To overcome this challenge, this paper introduces the "cloud control" photogrammetry technology to achieve fully automatic updates of orthophotos around long-distance pipelines, providing foundational data for the maintenance and inspection of these gas pipelines. This method replaces GCPs with images containing known orientation parameters, serving as control information. By matching tie points between new and old images, the "cloud control points" are transferred to the new images, enabling the image registration and production of orthophotos. The experiments conducted on the Fumin and Zhaotong segments of a long-distance gas pipeline in Yunnan Province demonstrate that, for UAV images with a ground resolution of 0.05 meters, using the "cloud control" method achieves a planar accuracy of 0.05 meters and an elevation accuracy of 0.07 meters. These results are comparable to the accuracy obtained by orienting the results using GCPs.

1. Instruction

With the ongoing global climate change, the development and use of clean energy have become a strategic focus for countries worldwide in addressing the energy crisis. Natural gas, as a clean energy source, is best transported through long-distance pipelines. Long-distance natural gas pipelines serve as crucial infrastructure for ensuring the distant transportation of natural gas, representing a significant initiative in addressing the uneven distribution and configuration of energy resources. As the natural gas industry rapidly expands, the safety of long-distance gas pipelines has become an increasingly important concern. In the event of a pipeline leak, not only does it pose a severe threat to the safety of nearby residents, but it also brings significant pollution to the surrounding environment, leading to incalculable losses for businesses (Chen et al., 2022). Therefore, obtaining and updating high-precision image data of the areas around long-distance gas pipelines in a timely manner is essential for detecting changes in high-consequence areas and strengthening the identification and risk management of such areas (Ma et al., 2011).

Maintenance and inspection of gas pipelines are primarily achieved through manual inspection and multi-sensor network inspection. However, given the extensive length and wide-ranging nature of long-distance gas pipelines, the maintenance and inspection tasks pose a considerable workload. To tackle this challenge, it is necessary to first identify areas of change, a task that can be accomplished by utilizing multiple sets of orthophotos generated by UAVs. Currently, there has been extensive research and application of using UAV photogrammetry to obtain geographic information. Wang (Wang et al., 2022) and Qin (Qin and Duan, 2023) have utilized UAVs and close-range photogrammetry for monitoring geological deformations, such as landslides. They generate detailed three-dimensional models using multiple UAV images and calculate the magnitude and direction of deformations for

monitoring and trend prediction. Wu (Wu et al., 2022) used UAV RGB photos to construct dense point clouds for estimating cotton plant height and the Leaf Area Index (LAI) after spraying defoliant, achieving dynamic monitoring of LAI changes in cotton at different stages. Lamsters, K. (Lamsters et al., 2022) performed two UAV surveys in 2019 and 2021 on a High-Arctic glacier in NW Svalbard and derived surface characteristics, elevation change, and velocity of High-Arctic Valley Glacier. Zanutta, A. (Zanutta et al., 2020) performed three multi-temporal UAV surveys using UAVs supported by GCPs to produce three-dimensional models to be used for comparison and validation. A multi-temporal analysis was carried out by gathering LiDAR dataset, regional technical cartography and orthophotos to monitor shoreline and beach changes.

In the production of UAV photogrammetry, due to the characteristics of small image footprints and significant geometric distortions of UAV images, the control orientation process typically requires a large number of control points. Although GNSS technology has reduced the difficulty of collecting GCPs, measuring these points in the field remains a challenging and time-consuming task. This results in the time spent measuring GCPs far exceeding the time required for image acquisition. Clearly, the measurement of GCPs remains a critical factor limiting the efficiency of aerial survey control orientation. Traditional "point control" photogrammetry is increasingly inadequate to meet the characteristics of image data in the era of big data and the requirements for processing efficiency and high automation. Addressing these shortcomings, this paper proposes an automatic updating method for orthophotos around long-distance gas pipelines based on "cloud control" photogrammetry (Zhang and Tao, 2017). Firstly, tie points are extracted from the newly acquired images. Then, the new images are corrected to a similar orientation as the old images based on the initial georeferencing information of the new images and the orientation parameters of known images.

Same-name points are extracted from the corrected images and the images with known orientation parameters. The object-space three-dimensional coordinates of the same-name points are calculated using multiple images with known orientation. Subsequently, the obtained same-name points are used as "cloud control points" for bundle block adjustment of the new images, achieving the orientation of the new images. Finally, a Digital Elevation Model (DEM) is produced using interpolation with tie points, and a new orthoimage is generated using an indirect method. This achieves the automatic updating of orthophotos without the need for GCPs. This paper introduces the application of "cloud control" technology to the production of orthophotos around long-distance gas pipelines for the first time, realizing large-scale fully automatic orthoimage updates. It improves the efficiency of acquiring geographic information around long-distance gas pipelines, providing crucial technical support for the regular maintenance and inspection of long-distance gas pipelines and the monitoring of high-consequence areas.

2. Methodology

2.1 "Cloud Control" Photogrammetry and Updating of Orthophoto

"Cloud Control" Photogrammetry is a novel photogrammetric method proposed by Professor Zhang Zuxun, a member of the Chinese Academy of Engineering at Wuhan University. It includes both "control data" and "processing technology". The former refers to existing geographic spatial information data,

LiDAR point clouds, and images with known orientation parameters, all of which are within a unified geographic spatial information framework. They form the "control framework" for the newly acquired image data. The latter involves constructing a space three-dimensional free network through matching between new images, as well as obtaining a large amount of dense control information for the free network of new images through matching with existing images or registration with other data within the control framework.

The essence of cloud control photogrammetry is to use spatial data with precise geographic information to replace the traditional use of GCPs to control images. Depending on the type of geographic spatial information data used, cloud control photogrammetry technology can be mainly categorized into image-based cloud control, vector-based cloud control, and LiDAR point cloud-based cloud control. UAVs can capture a large number of aerial images in the target area. After conventional photogrammetric production, these images become control data with geographic spatial information. By obtaining new images at different times within the same area, it is possible to achieve "cloud control" based on images through the matching relationship between new images and previously oriented images, as well as constructing a free network for new images.

In order to quickly update orthophotos around long-distance gas pipelines, this paper introduces the "cloud control" technology based on images with known orientation parameters. The technical route used is illustrated in Figure 1.
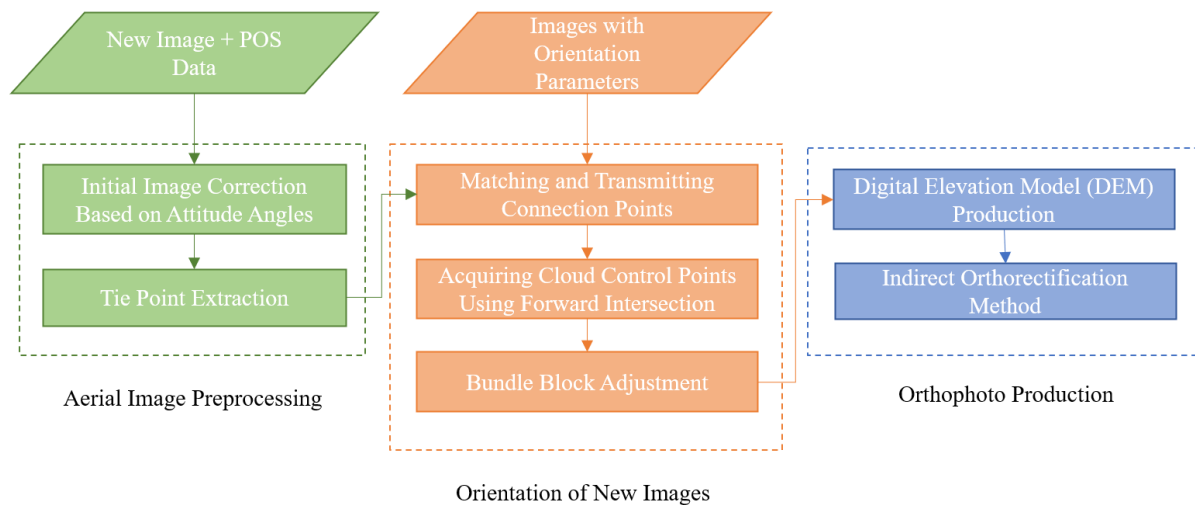

Figure 1. Technical route

2.2 Extraction of Tie Points Between New Images

Firstly, extract tie points with the same name between new images to establish connections between the images. We extract feature points for each newly acquired UAV image and then perform feature point matching. In this process, the Scale-invariant feature transform (SIFT) operator (Lowe, 2004) is used for feature point extraction. SIFT, proposed by David G. Lowe, is a classical algorithm for feature extraction and matching. It possesses scale and rotation invariance, making it effective for handling the characteristics of small UAV image footprints, significant differences in angles, and large variations in image content. We extract SIFT feature points for each image, obtaining 128-dimensional feature vectors for the feature points. Subsequently, in the adjacent area images of the

image where the matching feature points are located, we search for tie points with the same name. The Euclidean distance of feature vectors is used as the similarity measure for feature points. During the matching of tie points, Fast Library for Approximate Nearest Neighbors (FLANN) (Muja et al., 2009) is employed for fast search and matching of feature points. Finally, the matched tie points between images are filtered, and the Random Sample Consensus (RANSAC) algorithm (Fischler et al., 1981) is used to eliminate mismatches, achieving precise matching of feature points and extracting tie points between new images.

2.3 Matching Tie Points between New and Old Images

Images captured at different times may be obtained using

different remote sensing platforms and different flight plans, leading to significant differences in angles and scales between these images. When matching tie points between new and old images, these geometric differences can have a substantial impact. To minimize the influence of geometric differences on matching efficiency and accuracy, it is essential to calculate the projection transformation matrix between the new and old images for the same region based on the attitude parameters provided by the image's POS data. The new image is then resampled using the transformation matrix to correct it to the same viewpoint as the old image. Subsequently, a matching method combining the Harris operator (Harris et al., 1988) and normalization cross-correlation (NCC) (Lewis and John, 1995) is employed to extract tie points.

For each newly captured image, the GPS coordinates recorded during aerial photography are $(X_{gps}, Y_{gps}, Z_{gps})$, By traversing the oriented image information data, the image with known orientation parameters that is closest in Euclidean distance to the newly captured image is determined. If the orientation angles of the new and oriented images are denoted as $(\varphi_1, \omega_1, \kappa_1)$ and $(\varphi_0, \omega_0, \kappa_0)$ respectively, and the relative rotation angle is denoted as $(\varphi, \omega, \kappa)$, then $\varphi_0 - \varphi_1 = \varphi$, $\omega_0 - \omega_1 = \omega$, $\kappa_0 - \kappa_1 = \kappa$. If the coordinates of a pixel point in the new image are (x, y) and its corresponding coordinates in the corrected image are (x', y'), the mapping relationship between the corrected and uncorrected images can be established using Equation (1).

$$\begin{pmatrix} x \\ y \\ 0 \end{pmatrix} = R_\varphi R_\omega R_\kappa \begin{pmatrix} x' \\ y' \\ 0 \end{pmatrix} = \begin{pmatrix} \cos\varphi & 0 & -\sin\varphi \\ 0 & 1 & 0 \\ \sin\varphi & 0 & \cos\varphi \end{pmatrix} \begin{pmatrix} 1 & 0 & 0 \\ 0 & \cos\omega & -\sin\omega \\ 0 & \sin\omega & \cos\omega \end{pmatrix} \begin{pmatrix} \cos\kappa & -\sin\kappa & 0 \\ \sin\kappa & \cos\kappa & 0 \\ 0 & 0 & 1 \end{pmatrix} \begin{pmatrix} x' \\ y' \\ 0 \end{pmatrix} \tag{1}$$

Equation (1) can be simplified to Equation (2).

$$\begin{pmatrix} x \\ y \\ 0 \end{pmatrix} = R \begin{pmatrix} x' \\ y' \\ 0 \end{pmatrix} = \begin{pmatrix} \cos\varphi\cos\kappa - \sin\varphi\sin\omega\sin\kappa & -\cos\varphi\sin\kappa - \sin\varphi\sin\omega\cos\kappa & -\sin\varphi\cos\omega \\ \cos\omega\sin\kappa & \cos\omega\cos\kappa & -\sin\omega \\ \sin\varphi\cos\kappa + \cos\varphi\sin\omega\sin\kappa & -\sin\varphi\sin\kappa + \cos\varphi\sin\omega\cos\kappa & \cos\varphi\cos\omega \end{pmatrix} \begin{pmatrix} x' \\ y' \\ 0 \end{pmatrix} \tag{2}$$

Then:

$$\begin{pmatrix} x' \\ y' \\ 0 \end{pmatrix} = R^{-1} \begin{pmatrix} x \\ y \\ 0 \end{pmatrix} \tag{3}$$

After establishing the mapping relationship, bilinear interpolation is used to resample the new image, obtaining the corrected image.

Once the new image is corrected to the same viewpoint as the old image, tie points extracted from the new image are matched with tie points from multiple old images, and their object coordinates are obtained. The specific steps are as follows:
a) Based on the GPS information of the tie points in the image, search for UAV images in the old images that may contain tie points within a certain distance as the matching images.
b) Use the Harris feature extraction operator to extract a series of evenly distributed feature points in the matching images.
c) Establish a matching template with the tie points from the new image as the center, use the NCC algorithm to match tie points among the Harris corner points extracted from multiple matching images, and record their image coordinates.
d) If the tie points from the new image successfully match with two or more tie points in the oriented old images, known image coordinates of tie points, and the inner and outer orientation elements of the images, the object coordinates can be obtained in the old images using the multi-image forward intersection method.

2.4 "Cloud Control" Aerial Triangulation for New Images

After matching tie points between new and old images and obtaining the object coordinates in the old images, these tie points serve as "cloud control points" for the new images. Through the matching of tie points, a significant number of cloud control points can be generated. Using the object

coordinates of the cloud control points as known control data, the image coordinates of both the cloud control points and the tie points in the new images as observations, and the exterior orientation elements of the new images as unknowns, an error equation is established. Aerial triangulation is then performed for the survey area, and the solution of the error equation employs the Levenberg-Marquardt algorithm (LM) (Marquardt and Donald, 1963). The LM algorithm is a trust-region algorithm for solving nonlinear models and iteratively computes the optimal values of the exterior orientation elements for the new images.

Performing aerial triangulation on the new images using cloud control points with matching errors can affect the accuracy of the exterior orientation elements. To avoid mismatches, an iterative method is employed for gross error rejection of cloud control points. After each bundle adjustment, residuals for each cloud control point are computed. Points with large residuals are then removed, and the remaining cloud control points undergo a new round of bundle adjustment. This process is repeated until the desired accuracy is achieved. Finally, the exterior orientation elements for the new images are obtained.

2.5 Automatic Update of Orthophotos

After obtaining the orientation information for the new images, orthophotos are produced using the orientation results of the new images, achieving automatic updates of orthophotos in the study area. Based on a large number of tie points matched in the new images and their corresponding object coordinates, DEM data is generated through interpolation within predefined grid cells. Using the DEM data and image parameters, ground coordinates corresponding to pixel coordinates on the original images are determined using collinearity equations. For each

UAV image, orthorectification is performed pixel by pixel using the indirect method. If the ground coordinates of any point P on the orthophoto are (X, Y, Z), then its pixel coordinates on the original image are given by Equation (4):

$$
\left.
\begin{aligned}
x - x_0 &= -f \frac{a_1(X-X_S)+b_1(Y-Y_S)+c_1(Z-Z_S)}{a_3(X-X_S)+b_3(Y-Y_S)+c_3(Z-Z_S)} \\
y - y_0 &= -f \frac{a_2(X-X_S)+b_2(Y-Y_S)+c_2(Z-Z_S)}{a_3(X-X_S)+b_3(Y-Y_S)+c_3(Z-Z_S)}
\end{aligned}
\right\}
\tag{4}
$$

The pixel coordinates calculated for each point on the orthophoto may not be integer values. Bilinear interpolation is used to resample the images. Finally, all orthophotos in the survey area are stitched together and undergo radiometric and color balancing to produce a complete orthophoto product for the survey area.

3. Experiment

To validate the feasibility of the orthophoto automatic update method based on "cloud control" photogrammetry for pipelines, experiments were conducted in two segments around pipelines located in Fumin County and Zhaotong City, Yunnan Province, following the principles and processes of "cloud control" photogrammetry.

The first phase involved UAV photography of the target areas, adhering to photogrammetric production standards. External control points were collected, and DEM and orthophotos were generated, retaining the original image's interior and exterior orientation elements. After a certain period, the second phase of UAV photography was conducted in the target areas. Internal production was directly carried out during the second phase, using the first phase as the control source for "cloud control" photogrammetry. New orthophotos were produced in this process.

To validate accuracy, precision checks were performed using the control points from the first phase on the second phase data. A precision report was generated as a quality assessment for the second phase orthophoto production results. The entire experiment workflow is illustrated in Figure 2.
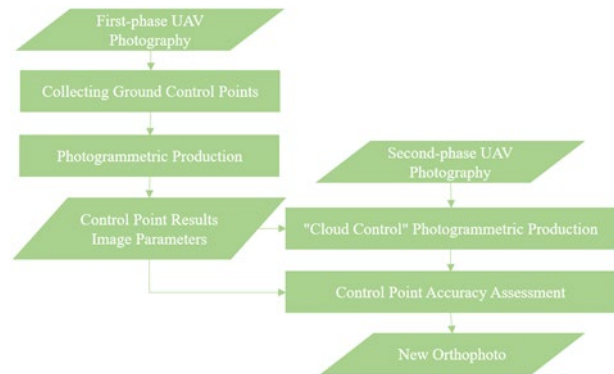

Figure 2. Experiment workflow

According to the experimental plan, photogrammetric production was initially carried out for the two sections of first-phase data. In the Fumin section, the first-phase data was captured in November 2018, with a total of 2 flight missions, acquiring 1881 UAV images, amounting to 56GB of data. The ground resolution of the images was 0.1 meters, covering an area of approximately 22 square kilometers. For the Zhaotong section, the first-phase data was captured in April 2021, with a total of 2 flight missions, acquiring 2672 UAV images, totaling 27.3GB of data. The ground resolution of the images was 0.05 meters, covering an area of about 2 square kilometers. Aerial triangulation was performed on both sets of data, and orthophotos were generated, as shown in Figures 3, 4, and 5.

(a)   (b)
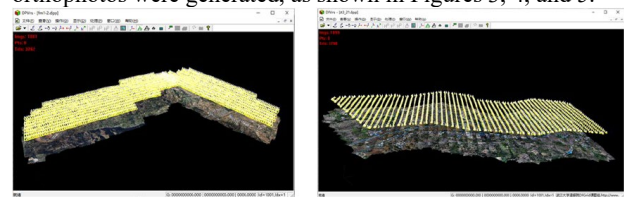
Figures 3. First-phase aerial triangulation results: (a) Fumin section, (b) Zhaotong section.

(a)   (b)

Figures 4. Distribution maps of selected control points: (a) Fumin section, (b) Zhaotong section.

(a)   (b)

Figures 5. First-phase orthophoto results: (a) Fumin section, (b) Zhaotong section.

Using the first-phase data as a reference, the second-phase "cloud control" photogrammetric production was conducted. In the Fumin section, the second-phase data was captured in August 2022, with a total of 5 flight missions, acquiring 18,072 UAV images, totaling 130GB of data. The ground resolution of the images was 0.05 meters, covering an area of approximately 18 square kilometers. For the Zhaotong section, the second-phase data was captured in August 2022, with a total of 5 flight missions, acquiring 1,300 UAV images, totaling 9.24GB of data. The ground resolution of the images was 0.04 meters, covering an area of about 1.8 square kilometers. The second-phase data for the Fumin section includes a larger number of images. To enhance processing efficiency and facilitate production, it was divided into 5 sub-projects based on flight missions. Both sets of data, using "cloud control" photogrammetry technology, underwent continuous iteration and outlier removal, resulting in the distribution of "cloud control points" as shown in Figure 6.
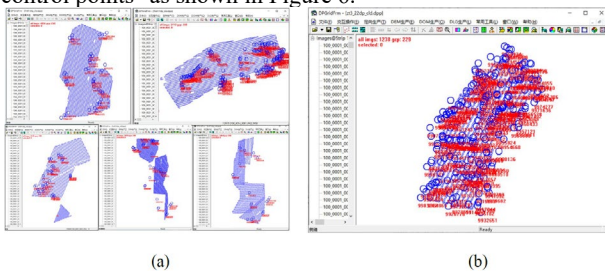

(a)   (b)

Figure 6. Distribution of "cloud control points" for the second-phase data: (a) Fumin section, (b) Zhaotong section.

Using the coordinates of the "cloud control points" as control conditions for the second-phase photogrammetric production, bundle adjustment was performed, and orthophoto production was conducted. The result is the generation of new orthophotos around the long-distance gas pipelines, as shown in Figure 7.
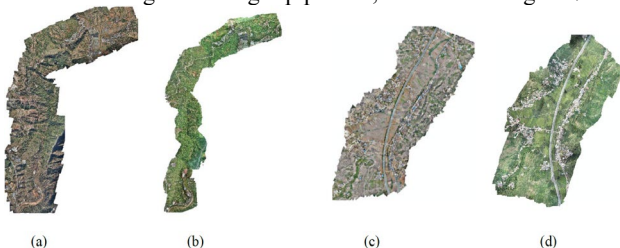

(a)   (b)   (c)   (d)

Figure 7. Orthophotos of the target area from two phases: (a) Fumin section in 2018, (b) Fumin section in 2022, (c) Zhaotong section in 2021, (d) Zhaotong section in 2022.

To verify the effectiveness of the second-phase orthophoto production, comparisons were made with the first-phase orthophotos, including overlay comparisons, change detection,

and mosaic comparisons, as shown in Figure 8. The two sets of UAV images were captured in different seasons, and the orthophotos reflect changes in vegetation and crops. Moreover, the fit is high in areas such as artificial structures. The differences between the two phases' orthophotos accurately reflect the changes in the long-distance gas pipelines and the surrounding areas.
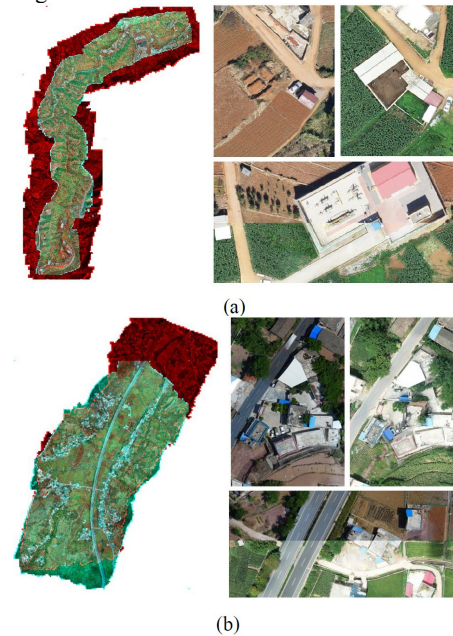

(a)

(b)

Figure 8. Partial results of overlay comparison, change comparison, and mosaic comparison of the two-phase orthophotos: (a) Fumin section, (b) Zhaotong section.

Using the GCPs collected during the first-phase photogrammetric survey for accuracy verification, the precision reports for the second-phase orthophotos are presented in Tables 1 and 2.

Point ID	Dx(m)	Dy(m)	Dz(m)
9900008	0.003	0.073	-0.310
9900030	0.104	0.003	0.485
9900022	0.184	-0.163	-0.108
9900044	-0.062	0.028	0.193
9900066	0.000	0.018	0.386
9900048	0.141	-0.004	0.062
9900072	-0.045	0.019	0.264
9900059	0.012	0.181	-0.251
9900081	0.009	-0.069	-0.054
RMS	DXDY：0.098		DZ：0.301

Tables 1. The accuracy check results for the checkpoint in the second-phase orthophoto of the Fumin section

Point ID	Dx(m)	Dy(m)	Dz(m)
8800031	-0.127	0.047	0.463
8800033	-0.095	0.054	0.204
8800035	-0.094	-0.173	-0.242
8800037	-0.210	-0.016	0.580
8800058	-0.026	-0.054	0.887
8800085	-0.111	-0.034	-0.619
8800041	0.236	0.045	0.270
8800038	0.073	0.035	-0.216
8800051	0.105	0.052	0.386
RMS	DXDY：0.101		DZ：0.299

Tables 2. The accuracy check results for the checkpoint in the second-phase orthophoto of the Zhaotong section

The accuracy report indicates that the planimetric accuracy of

the second-phase orthophotos in both the Fumin and Zhaotong sections is 0.1 meters, and the elevation accuracy is 0.3 meters.

4. Conclusion

In addressing the efficiency challenges of producing orthophotos based on external control points for the maintenance and inspection of long-distance gas pipelines, this study applied "cloud control" photogrammetry technology to update aerial images around the gas pipelines. Experiments were conducted in the Fumin and Zhaotong sections of a long-distance gas pipeline in Yunnan Province. The results demonstrate that using historical images with accurate orientation parameters for the same surveyed area, the orientation and orthophoto production of new images were achieved solely through UAV photography without ground control point collection. The orthophotos processed using "cloud control" technology met the accuracy criteria of relative accuracy better than 2 pixels, making them suitable for practical production and holding significant application value.

Acknowledgements

References

Chen, K., Shi, N., Lei, Z., Chen, X., Qin, W., Wei, X., Liu, S., 2022. Risk Classification of Shale Gas Gathering and Transportation Pipelines Running through High Consequence Areas. *Processes*, 10(5), 923.

Fischler, M. A., Bolles, R. C., 1981. Random sample consensus: a paradigm for model fitting with applications to image analysis and automated cartography. *Communications of the ACM*, 24(6), 381–395.

Harris, C., Stephens, M. et al., 1988. A combined corner and edge detector. *Alvey vision conference*, 15number 50, Citeseer, 10–5244.

Lamsters, K., Ješkins, J., Sobota, I., Karušs, J., Dzerin¸sˇ, P., 2022. Surface characteristics, elevation change, and velocity of high-arctic valley glacier from repeated high-resolution UAV photogrammetry. *Remote Sensing*, 14(4), 1029.

Lewis, J. P., 1995. Fast normalized cross-correlation. *Vision interface*, 10number 1, 120–123.

Lowe, D. G., 2004. Distinctive image features from scale-invariant keypoints. *International journal of computer vision*, 60, 91–110.

Ma, J., Chen, L., Zhang, P. D., Wang, S., 2011. High consequence areas (hcas) assessment for long-distance oil/gas pipeline. *ICPTT 2011: Sustainable Solutions For Water, Sewer, Gas, And Oil Pipelines*, 1740–1748.

Marquardt, D. W., 1963. An algorithm for least-squares estimation of nonlinear parameters. *Journal of the society for Industrial and Applied Mathematics*, 11(2), 431–441.

Muja, M., Lowe, D. G., 2009. Fast approximate nearest neighbors with automatic algorithm configuration. *VISAPP (1)*, 2(331-340), 2.

Qin, Y., Duan, Y., 2023. A METHOD FOR MEASURING LARGE-SCALE DEFORMATION OF LANDSLIDE BODIES BASED ON NAP-OF-THE-OBJECT PHOTOGRAMMETRY. *The International Archives of the Photogrammetry, Remote Sensing and Spatial Information Sciences*, 48, 29–35.

Wang, Y., Duan, Y., Pang, B., Liu, R., 2022. The key technologies of geological disaster dynamic monitoring based on nap-of-the-object photogrammetry. *ISPRS Annals of the Photogrammetry, Remote Sensing and Spatial Information Sciences*, 10, 171–176.

Wu, J., Wen, S., Lan, Y., Yin, X., Zhang, J., Ge, Y., 2022. Estimation of cotton canopy parameters based on unmanned aerial vehicle (UAV) oblique photography. *Plant Methods*,18(1), 129.

Zanutta, A., Lambertini, A., Vittuari, L., 2020. UAV photogrammetry and ground surveys as a mapping tool for quickly monitoring shoreline and beach changes. *Journal of Marine Science and Engineering*, 8(1), 52.

Zuxun, Z., Pengjie, T., 2017. An overview on "cloud control" photogrammetry in big data era. *Acta Geodaetica et Cartographica Sinica*, 46(10), 1238.